Article:
Llanos-Expósito, M., Benito, J., Fraile, L. M. et al. (2025) Structure of 128Sn selectively populated in the $beta$ decay of the 128In ground state. Physical Review C. 064310. ISSN: 2469-9993

https://doi.org/10.1103/PhysRevC.111.064310

Structure of ^{128}Sn selectively populated in the β decay of the ^{128}In ground state

M. Llanos-Expósito,[1,*] J. Benito,[1,2,3,†] L. M. Fraile,[1,‡] A. Illana,[1,4,5,§] J. Acosta,[6] A. Algora,[7] B. Andel,[8] A. N. Andreyev,[9,10] S. Antalic,[8] M. Araszkiewicz,[11] R. A. Bark,[12] C. Bernerd,[10] N. Bernier,[13,14] B. Bhengu,[15] D. Bittner,[16] M. J. G. Borge,[6] J. A. Briz,[1] K. Chrysalidis,[10] T. E. Cocolios,[17] C. Costache,[18] J. G. Cubiss,[9,10] U. Datta,[19] H. De Witte,[17] N. Encina,[1] A. Esmaylzadeh,[16] Z. Favier,[10] D. Fernández,[6] C. Ferrera,[6] H. O. U. Fynbo,[20] V. García-Távora,[6] G. Georgiev,[21] M. Górska,[22] R. Heinke,[10] J. L. Herraiz,[1] P. M. Jones,[12] J. Jolie,[16] D. S. Judson,[23] A. Jungclaus,[6] M. Karny,[11] A. Korgul,[11] U. Köster,[24,10] Th. Kröll,[25] M. Labiche,[26] S. Lalkovski,[27] B. Lesch,[13] M. Ley,[16] R. Lică,[10,18] M. Madurga,[28] N. Mărginean,[18] B. A. Marsh,[10,‖] K. Miernik,[11] C. Mihai,[18] M. Mikolajczuk,[11,22] J. Mišt,[8] J. R. Murias,[1] E. Nácher,[7] C. Neacsu,[18] V. M. Nouvilas,[1] S. Ntshangase,[15] B. Olaizola,[6,10] J. N. Orce,[13] C. A. A. Page,[9,10] R. D. Page,[23] J. Pakarinen,[4,5] P. Papadakis,[26] A. Perea,[6] M. Piersa-Siłkowska,[10] Zs. Podolyak,[10,29] J.-M. Régis,[16] J. Rog,[11] S. Rothe,[10] B. Rozwoda,[11] V. Sánchez-Tembleque,[1,30] K. Solak,[11] S. Stegemann,[10] M. Stepaniuk,[11] A. Stoica,[18] M. Stryjczyk,[4,5] O. Tengblad,[6] A. Turturica,[18] G. Turturica,[18] J. M. Udías,[1] S. Ujeniuc,[18] P. Van Duppen,[17] Ir. Vasilev,[27] M. von Tresckow,[25] N. Warr,[16,23] Z. Yue,[9,10] and S. Zajda[11]

(IDS collaboration)

[1]*Grupo de Física Nuclear, EMFTEL & IPARCOS, Universidad Complutense de Madrid, CEI Moncloa, E-28040 Madrid, Spain*
[2]*Dipartimento di Fisica and INFN, Sezione di Padova, I-35131 Padova, Italy*
[3]*INFN Laboratori Nazionali di Legnaro, I-35020 Legnaro, Italy*
[4]*University of Jyväskylä, Department of Physics, P.O. Box 35, FI-40014 Jyväskylä, Finland*
[5]*Helsinki Institute of Physics, University of Helsinki, FI-00014 Helsinki, Finland*
[6]*Instituto de Estructura de la Materia, CSIC, E-28006 Madrid, Spain*
[7]*Instituto de Física Corpuscular, CSIC-Universidad de Valencia, E-46071 Valencia, Spain*
[8]*Department of Nuclear Physics and Biophysics, Comenius University in Bratislava, SK-84248 Bratislava, Slovakia*
[9]*School of Physics, Engineering and Technology, University of York, York YO10 5DD, United Kingdom*
[10]*CERN, CH-1211 Geneva 23, Switzerland*
[11]*Faculty of Physics, University of Warsaw, PL 02-093 Warsaw, Poland*
[12]*iThemba LABS, National Research Foundation, P.O. Box 722, Somerset West 7129, South Africa*
[13]*Department of Physics & Astronomy, University of the Western Cape, P/B X17, Bellville 7535, South Africa*
[14]*National Institute for Theoretical and Computational Sciences (NITheCS), University of Stellenbosch, Private Bag X1, Matieland 7602, South Africa*
[15]*Department of Physics & Engineering, University of Zululand, Private Bag X1001, KwaDlangezwa 3886, South Africa*
[16]*Institut für Kernphysik, Universität zu Köln, D-50937 Köln, Germany*
[17]*KU Leuven, Instituut voor Kern- en Stralingsfysica, B-3001 Leuven, Belgium*
[18]*"Horia Hulubei" National Institute of Physics and Nuclear Engineering, RO-077125 Bucharest, Romania*
[19]*Saha Institute of Nuclear Physics, HBNI, 1/AF Bidhannagar, Kolkata 700064, India*
[20]*Department of Physics and Astronomy, Aarhus University, DK-8000 Aarhus C, Denmark*
[21]*IJCLab, IN2P3-CNRS, Université Paris-Saclay, F-91405 Orsay, France*
[22]*GSI Helmholtzzentrum für Schwerionenforschung, Planckstraße 1, D-64291 Darmstadt, Germany*
[23]*Department of Physics, Oliver Lodge Laboratory, University of Liverpool, Liverpool L69 7ZE, United Kingdom*
[24]*Institut Laue Langevin, 71 Avenue des Martyrs, F-38000 Grenoble, France*
[25]*Institut für Kernphysik, Technische Universität Darmstadt, D-64289 Darmstadt, Germany*
[26]*STFC Daresbury Laboratory, Daresbury, Warrington WA4 4AD, United Kingdom*
[27]*Faculty of Physics, Sofia University, St. Kliment Ohridski, Sofia, Bulgaria*

[*]Contact author: marcllan@ucm.es
[†]Contact author: jabenito@ucm.es
[‡]Contact author: lmfraile@ucm.es
[§]Contact author: andres.illana@ucm.es
[‖]Deceased.

[28]*Department of Physics and Astronomy, University of Tennessee, Knoxville, Tennessee 37996, USA*
[29]*Department of Physics, University of Surrey, Guildford GU2 7XH, United Kingdom*
[30]*HES-SO, HEPIA, CH-1202 Geneva, Switzerland*

(Received 17 January 2025; accepted 12 May 2025; published 10 June 2025)

High-resolution γ-ray spectroscopy and fast-timing methods were employed to study the excited structure of ^{128}Sn, populated via the β-decay chain of ^{128}Cd $\rightarrow$ ^{128}In $\rightarrow$ ^{128}Sn. The experiment was performed by online mass separation at the ISOLDE facility at CERN, profiting from intense and pure Cd beams obtained by a temperature-controlled quartz transfer line combined with resonant laser ionization. An extended ^{128}Sn level scheme populated in the β^- decay of the low-spin ^{128}In isomer was constructed, adding a total of 81 new γ-ray transitions and 30 new levels. Lifetimes of excited states were measured using time-delayed $\beta\gamma(t)$ and $\gamma\gamma(t)$ coincidences. The lifetime of the (4^+) state was measured for the first time, making it possible to deduce the $B(E2; 4^+ \rightarrow 2^+)$ transition strength. The previously measured (5^-) state was reassessed with improved statistics. Additionally, an upper limit for the lifetime of the state at 2378 keV was established. The derived reduced transition probabilities support a tentative spin-parity assignment of (4^-) for this level. The experimental level scheme and transition probabilities are compared with available shell-model calculations.

DOI: 10.1103/PhysRevC.111.064310

I. INTRODUCTION

The region around the exotic doubly magic ^{132}Sn isotope is one of the most thoroughly studied since it is within reach of current experimental facilities [1–3]. The understanding of nuclear structure requires the systematic investigation of nuclei near the $Z = 50$ and $N = 82$ shell closures, where collective effects emerge with only a few extra nucleons. Shell-model calculations have been developed to describe the nuclear structure around ^{132}Sn [4,5], achieving a rather good agreement, particularly below the $N = 82$ shell gap.

In spite of being just four neutrons lighter than ^{132}Sn, the structure of ^{128}Sn has not been experimentally explored in sufficient detail. In particular, reduced transition probabilities remain largely unmeasured, despite their importance for testing nuclear wave functions through excited-state lifetime measurements.

Early relevant publications on ^{128}Sn are based on β-decay experiments at the OSIRIS ISOL facility in Studsvik (Sweden) by Fogelberg *et al.* [6,7], using a mass-separated $A = 128$ beam containing Cd, In, Sn, Sb, and Ag isobars. Several γ rays following the β decay of both the (3^+) ^{128g}In ground state (g.s.) and (8^-) ^{128m1}In isomer are reported, populating levels up to 4510 and 4898 keV, respectively. It should be noted that the Q_{β^-} value is 9171(18) keV, while the neutron separation energy is 7963(20) keV [8]. A strongly fed (7^-) state at 2091 keV with $T_{1/2} = 6.5(5)$ s was identified in the β^- decay of the (8^-). The population of the (5^-) and (7^-) negative-parity states in Ref. [6] was somewhat uncertain due to the difficulty in obtaining sources where ^{128}In and ^{128}Sn were in equilibrium. Their placement in the decay scheme is doubtful, indicating the need for a reevaluation of the ^{128}In $\rightarrow$ ^{128}Sn decay. Multipolarities of low-lying transitions were obtained from internal conversion electron measurements [6,7]. Furthermore, lifetime measurements using plastic and NaI(Tl) scintillators are also provided in Ref. [6] for the 2121-keV state, yielding $T_{1/2} = 8.6(8)$ ns. In addition, the 2492-keV level half-life was measured, giving a value of $T_{1/2} = 2.91(14)$ µs [9].

A more recent investigation of the high-spin (16^+) isomeric state in ^{128m2}In, performed at the IGISOL facility with JYFLTRAP purification, identified a (15^+) state in ^{128}Sn at ≈5.8 MeV [10,11]. This state decays via a 1779-keV γ ray to the known (15^-) isomer at 4099.5 keV [$T_{1/2} = 220(30)$ ns], already reported in fragmentation [12] and heavy-ion fusion-fission reactions [13], and interpreted as a seniority-4 $\nu h_{11/2}^{-3} d_{3/2}^{-1}$ configuration.

This work presents the study of ^{128}Sn levels populated in the β-decay chain ^{128}Cd $\rightarrow$ ^{128}In $\rightarrow$ ^{128}Sn. Out of the three known β-decaying states in ^{128}In, the (3^+) g.s., the low-lying (8^-) isomer, and the (16^+) isomer at 1.8 MeV, this measurement benefits from the selective population of the low-spin ground state of ^{128}In in the β decay of the ^{128}Cd 0^+ state. The analysis is focused on two fundamental aspects: the potential misplacement of transitions in the ^{128}In decay scheme and the limited knowledge of lifetimes and transition probabilities in ^{128}Sn. To this end, a detailed study of the β decay of the ^{128}In (3^+) g.s. has been performed. Furthermore, the difference in half-lives between ^{128}Cd and ^{128}In facilitates a clear separation of their respective decay activities. The results provide new insights into the nuclear structure of ^{128}Sn and enable a reevaluation of the ^{128}In decay scheme.

The remainder of this paper is organized as follows. Details on the experimental method used in the present work are provided in Sec. II. The experimental results are presented in Sec. III. and discussed in Sec. IV. Conclusions are drawn in Sec. V.

II. EXPERIMENTAL DETAILS

The nuclei in the $A = 128$ β-decay chain were populated at ISOLDE/CERN facility starting from a high-purity ^{128}Cd ion beam. Uranium-carbide/graphite (UC_x) was employed as

target material. Protons from the CERN PS Booster accelerated to 1.4 GeV induced spallation reactions in a tungsten rod below the target container. The generated fast neutrons induced fission in the target and aided in suppressing contamination from neutron-deficient species, compared to direct production with protons. A temperature-controlled quartz transfer line between the target and the ion source acted as a chemical selector, due to strong adsorption of cesium and indium [14], thus effectively reducing the unwanted products [15,16]. The use of laser ionization via the Resonance Ionization Laser Ion Source (RILIS) [17] enabled selective ionization of cadmium with high efficiency [18]. Mass separation was achieved with the General Purpose Separator (GPS). As a result, a ^{128}Cd beam with a yield of $\approx 1.6 \times 10^4$ ions/μC was obtained, with a suppression factor of isobaric contaminants larger than 3000 for ^{128}Cs and in excess of 400 for ^{128}In [19].

The cadmium ions were guided to the center of the experimental setup at the ISOLDE Decay Station (IDS) where the ion beam was implanted on a movable tape. The beam implantation was controlled by an electrostatic beam gate, starting 5 ms after each proton pulse and lasting for 500 ms. At IDS, an array of six high-purity germanium (HPGe) clover detectors with a combined full-energy peak efficiency of 6.0(2)% at 1 MeV was used. Three β detectors surrounded the implantation point in the tape with a 44(2)% combined β efficiency. Two of them consisted of EJ-232Q plastic scintillators coupled to silicon photomultipliers while the third one was an ultrafast 3-mm-thick NE111A plastic scintillator attached to a fast photomultiplier tube (PMT). The latter, in combination with two $LaBr_3$(Ce) crystals with the shape of truncated cones [20] fitted with fast PMTs [21], was also employed for fast-timing measurements [22–24]. A XIA Pixie16 data acquisition (DAQ) system was used to digitize the detector signals. The fast-timing signals were subject to analog processing via constant fraction discriminators and time-to-amplitude converters prior to being fed to the digitizers, while slow and logic signals were directly input to the DAQ.

The time response calibration of $LaBr_3$(Ce) detectors was performed by constructing the full-energy peak (FEP) walk curve, which corrects the time response as a function of energy. This was achieved using $\beta\gamma(t)$ and $\gamma\gamma(t)$ coincidences with ^{140}Ba, ^{152}Eu, ^{138}Cs, and ^{88}Rb calibration sources. For further details about the detection setup and calibration procedures, the reader is referred to Ref. [19].

III. EXPERIMENTAL RESULTS

This work focuses on the γ and fast-timing investigation of the excited structure of ^{128}Sn populated in the β decay of the ^{128}In (3^+) g.s. The two other β-decaying higher-lying ^{128}In isomers [6,10] are not populated in the decay of the ^{128}Cd 0^+ ground state.

The implantation tape was moved every 38.4 s to avoid the buildup of long-lived activities. Since the β-decay half-life of ^{128}Sn is 59.07(14) min [25], the analyzed data mostly contain the decays of ^{128}Cd and ^{128}In. By turning the RILIS ionization off, the release of surface-ionized ^{128}In was cross-checked, and it was found to be well below 1% of the total beam [19].

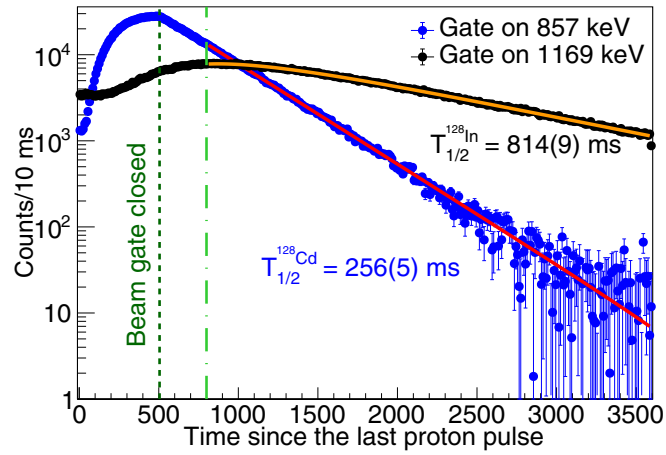

FIG. 1. Time distribution analysis of the ^{128g}Cd 0^+ (blue curve) and ^{128g}In (3^+) (black curve) β-decay half-lives and decay fit curves. The dark green vertical dashed line represents the end of the implantation. The start of the region considered for the fit is indicated with a light green dot-dashed line. Time distributions gated on 1169- and 857-keV transitions are shown. The final values adopted for ^{128g}Cd and ^{128g}In β-decay half-lives obtained from the weighted average of several transitions are shown in the plot (see text for details).

The β-delayed neutron emission from the ^{128}In g.s. is very small, with $P_n = 3.84(36) \times 10^{-2}$% [26,27], so the vast majority of the β decay feeds ^{128}Sn. No γ transitions have been observed from the βn-decay branch.

The time distribution of the two most intense γ-ray transitions observed is plotted in Fig. 1, reflecting the different β-decay lifetimes convoluted with the implantation profile and the characteristic release time structure arising from the pulsed proton beam at ISOLDE. Owing to the large difference in the half-lives of 246(2) and 816(27) ms, respectively [25], it is possible to unambiguously identify most of the γ rays from the ^{128}Cd and ^{128}In decays. In addition, the identification of the γ transitions in ^{128}Sn is based on $\gamma\gamma$ coincidences with previously known transitions.

A. Half-life of ^{128g}In (3^+)

The ^{128g}Cd and ^{128g}In β-decay half-lives were measured by fitting the time distributions relative to the proton pulse impact (Fig. 1). Due to the high instantaneous decay rate, dead time effects are present just after the implantation. Therefore, the starting point of the time window for the fit has been optimized by employing a χ^2 test, leading to an optimal 800 ms. The end of the fit range is defined by the 3600 ms minimum time between implantation, which corresponds to 14 half-lives of ^{128}Cd and 4 half-lives of ^{128}In.

The β-decay half-life of ^{128g}Cd was determined by fitting an exponential decay function with a constant background, selecting the full-energy peaks of the most intense 315-, 857-, and 935-keV γ rays, with Compton background subtracted. For each of the transitions, a probability distribution was created by sampling both the fit range and data binning, and

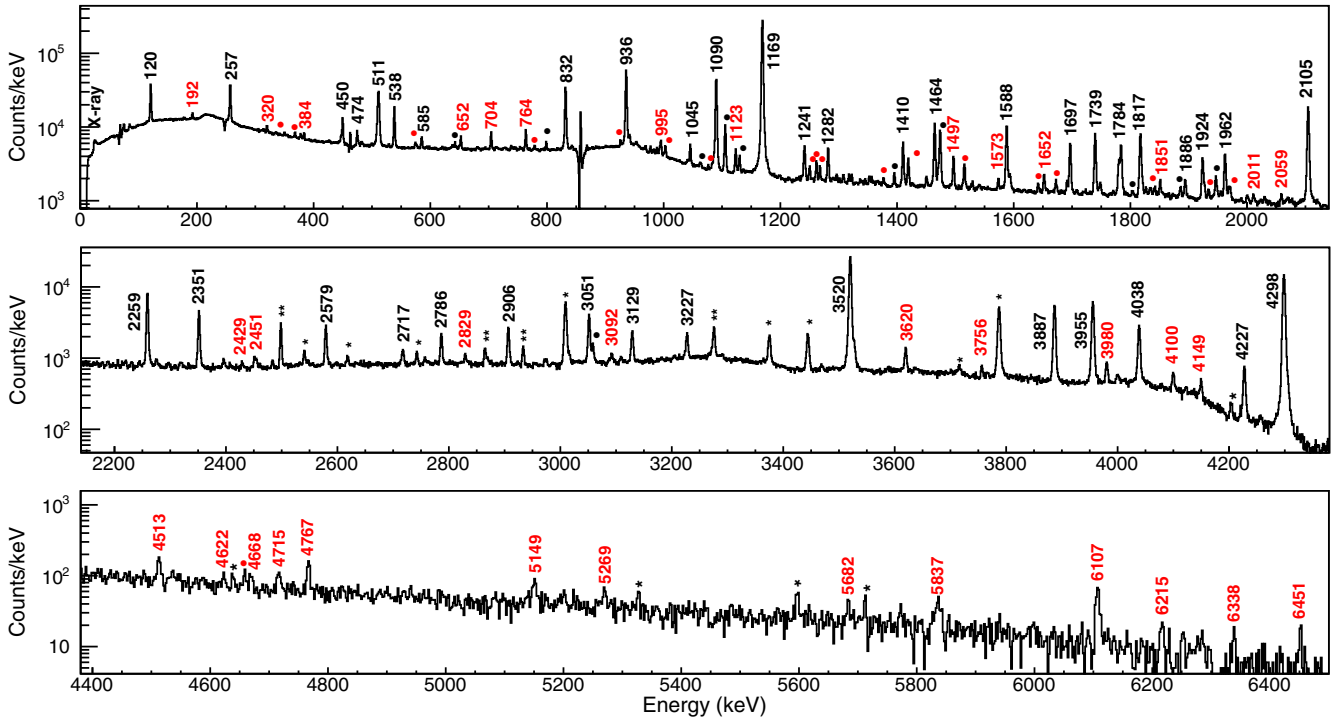

FIG. 2. β-gated γ-ray energy spectrum recorded following the decay of ^{128}Cd. The spectrum is constructed with a time window since proton impact and subtraction of long-lived to observe only γ rays from the β decay of ^{128g}In $\rightarrow$ ^{128g}Sn. The negative counts at 857 keV arise from oversubtraction of the most intense ^{128}Cd full-energy peak. The previously known γ rays are labeled in black when the label size allows it; otherwise, only black solid circles are shown. The new transitions identified in this work are labeled in red or marked with red solid circles. Single- and double-escape peaks are labeled with $*$ and $**$, respectively.

the uncertainty was calculated as its standard deviation. The final value was obtained by a weighted mean of the three individual values with a coverage factor of 2σ, yielding a half-life of $T_{1/2} = 256(5)$ ms. The result is in agreement with the recently measured 243(11) ms ^{128g}Cd half-life [28] and within 2σ from the $T_{1/2} = 246(2)$ ms value reported in the latest evaluation [25].

In the case of ^{128g}In, a function corresponding to the solution of the Bateman equations [29] for a two-step decay chain was employed. The lifetime of ^{128g}Cd was fixed to the measured value discussed above, taking into account its uncertainty. The procedure was applied to the 1169-, 936-, 1090-, and 2105-keV γ rays, using the same procedure as above. The final value was obtained from the weighted average, giving $T_{1/2} = 814(9)$ ms. The result is in agreement with $T_{1/2} = 816(27)$ ms from the latest evaluation [25].

B. Level scheme of ^{128}Sn

A β-gated γ-ray spectrum is presented in Fig. 2. The spectrum was constructed to ensure that only γ rays belonging to ^{128g}In decay were selected, by selecting a time window of 130 to 740 ms relative to the proton impact (see Fig. 1) and subtracting contributions of γ rays associated with ^{128}Cd decay using a 30 to 51 ms range. In this way, γ transitions in ^{128}Sn can be identified up to 6.4 MeV.

The ^{128g}In decay scheme to ^{128}Sn has been built based on $\gamma\gamma$ coincidences and intensity balance. As an example, the γ-ray spectrum in coincidence with the intense 1169-keV $2^+ \rightarrow 0^+$ transition is shown in Fig. 3 above 2500 keV, illustrating previously unobserved peaks at high energies. The observed coincidences with the 1357-keV γ ray, assigned to the $(2^+) \rightarrow (0_2^+)$ transition (see Sec. IV) are presented in Fig. 4. The level scheme includes previously known levels and γ transitions [6,7] with the addition of 81 new γ transitions and 30 new states. The expanded level scheme is shown in

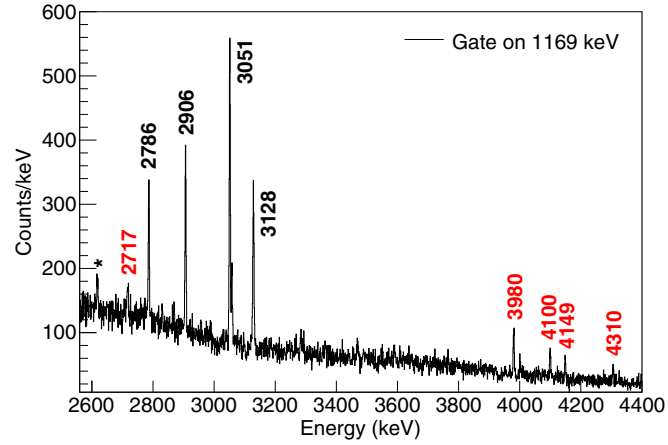

FIG. 3. Compton-subtracted γ-γ energy projection spectrum gated on the 1169-keV $2^+ \rightarrow 0^+$ transition in ^{128}Sn in the 2600–4400 keV high energy range. The previously known γ rays are labeled with their energies in black, while new ones are marked in red. The 3128-keV single-escape peak is labeled with an asterisk.

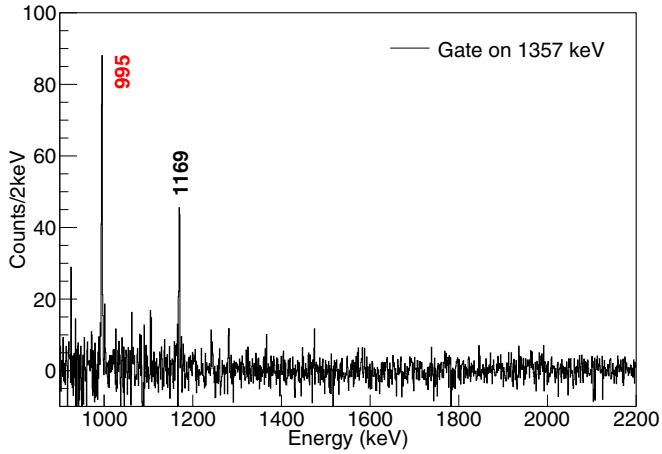

FIG. 4. Compton-subtracted γ-γ energy projection spectrum gated on the 1357-keV $(2^+)\rightarrow(0_2^+)$ transition in ^{128}Sn in the 940–2200 keV energy range. The new coincident 995-keV γ ray is labeled in red.

Figs. 5 and 6. A list of γ rays, along with their corresponding intensities, is provided in Table I with the deexcited and populated states.

The β-decay feeding has been determined from the intensity balance between feeding and depopulating γ rays for each level. Since the β decay of the (3^+) ^{128}In g.s. to the 0^+ ^{128}Sn g.s. would be via a second-forbidden transition, direct β feeding to the g.s. has been taken to be zero. Apparent $\log ft$ values are derived assuming allowed transitions [30] from γ-ray intensities corrected for internal conversion [31], the Q_{β^-}, and the measured β-decay half-life.

C. Lifetimes of excited states in ^{128}Sn

Lifetimes of excited states in ^{128}Sn in the nanosecond and subnanosecond ranges have been investigated via $\beta\gamma\gamma(t)$, $\beta\gamma(t)$, and $\gamma\gamma(t)$ fast-timing methods [3,22–24,32]. The half-lives of the 2378-keV state, 2121-keV (5^-) state, and 2001-keV (4^+) state are discussed.

The time-delayed spectrum for the analysis of the lifetime of the 2121-keV state, with a proposed (5^-) spin-parity (see Sec. IV) is displayed in Fig. 7. The half-life was obtained from $\beta\gamma(t)$ events time selected for the ^{128}In decay, and measured by summing the 120-, 832-, and 1169-keV full-energy peaks in the two $LaBr_3$(Ce) detectors. The half-life was measured by fitting the delayed slope of the combined spectra once the influence of Compton events under the peaks is taken care of [33]. Neither the population of known isomeric states nor evidence of an unknown isomeric state that may feed the (5^-) level was observed. An exponential decay plus a constant background fit results in $T_{1/2} = 10.5(3)$ ns. The resulting half-life is larger than the previously measured value, $T_{1/2} = 8.6(8)$ ns, using NaI(Tl) detectors [6].

The lifetime of the 2001-keV (4^+) state was measured from the time-delayed coincidences between the two $LaBr_3$(Ce). No prior lifetime measurement was reported in the literature. This level is almost entirely fed by γ transitions ($I_\beta < 0.9\%$). Besides, almost all the feeding is provided by the 120-keV transition from the long-lived (5^-) state with $T_{1/2} = 10.5(3)$ ns. Thus, the analysis was performed using time difference information between the two $LaBr_3$(Ce) detectors. In this manner, the (5^-) level half-life does not affect the measurement. An extra condition in the time to amplitude converter (TAC) β-$LaBr_3$(Ce) was required by including only β-delayed events by more than 2 ns relative to the $\beta\gamma$ prompt. This suppresses most of the γ rays, leaving only the 120-832-1169 cascade peaks below the (5^-) state in the spectra. The lifetime analysis of the 2001-keV state is shown in Fig. 8. A mean lifetime of $\tau = 25(13)$ ps, which translates to $T_{1/2} = 17(9)$ ps, was obtained from the centroid shift method [22,23,32,34].

The lifetime analysis of the 2378-keV level is depicted in Fig. 9. In this case, $\beta\gamma\gamma(t)$ events are used to study the time-difference distribution of the 257-keV γ ray in the $LaBr_3$(Ce) detectors vs the β events, with an extra coincidence condition on the 120-keV transition in the HPGe detectors. The time distribution does not have a delayed component, which is characteristic of a short lifetime. Unfortunately, the centroid shift method could not be employed because no independent time reference was found. Instead, the half-life was measured from a fit to a Gaussian convoluted with an exponential function, by probing different half-life values while evaluating the χ^2/NDF. An upper limit of $T_{1/2} \leqslant 40$ ps was adopted from the $T_{1/2}$ value given by $(\chi^2_{\rm min}+1)$/NDF. Additionally, the 329-keV γ-ray deexciting the 2412-keV 3^+ state ($\tau = 1.3(4)$ ps) from the ^{140}Ba calibration source was used to verify the prompt $\beta\gamma(t)$ behavior at close energies.

Reduced transition probabilities $B(X\lambda)$ for transitions in ^{128}Sn were calculated from the measured lifetimes of the (4^-), (5^-), and (4^+) levels, the γ-ray intensities, and the tabulated internal conversion coefficients [31] assuming pure multipolarities. The results are summarized in Table II.

IV. DISCUSSION

Tentative spin-parity assignments for the populated states in ^{128}Sn are based on the β-decay selection rules, the observed γ transitions between levels, and the transition probabilities provided by the lifetime measurements. The starting point is the proposed (3^+) g.s. for ^{128}In, interpreted as a member of the $\pi g_{9/2}^{-1}\nu d_{3/2}^{-1}$ multiplet [36,37], and the previous information about ^{128}Sn [6].

The systematics of excited states in even-even Sn isotopes is shown in Fig. 10, including the 2^+, 4^+, and 6^+ yrast states, the second 0^+ and 2^+ states, and the low-lying 4^-, 5^-, 6^-, and 7^- levels.

Shell-model calculations for states for ^{128}Sn are discussed in Refs. [38–41]. Reference [38] uses ^{132}Sn as a core and employs the $2s_{1/2}$, $1d_{5/2}$, $1d_{3/2}$, $0g_{7/2}$, and $0h_{11/2}$ orbits as valence space where neutrons are holes and protons are particles. An effective interaction is derived employing perturbative many-body techniques starting from a free nucleon-nucleon interaction. Teruya *et al.* [39] adopt the same model space with all five single-particle orbitals in the 50–82 major shell, with a phenomenological interaction with two-body terms

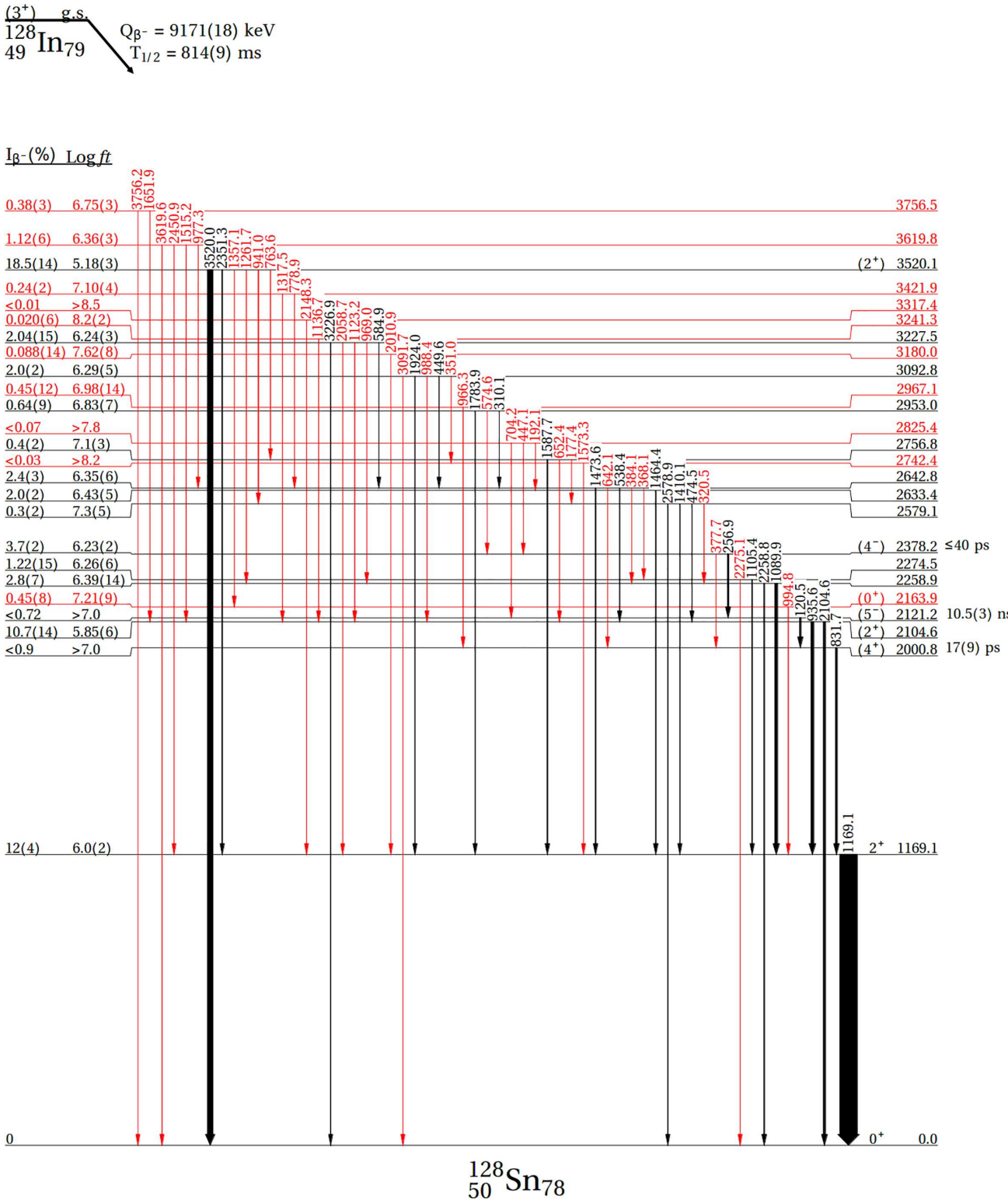

FIG. 5. Level scheme of ^{128}Sn observed following the β decay of the ^{128g}In (3^+) state. Levels and transitions previously identified are colored in black, while those newly identified in this work are highlighted in red. Transition widths are proportional to their relative intensities.

consisting of pairing and quadrupole-quadrupole interactions. The same model space and a similar approach are adopted in Ref. [40] by using the $jj55$ interaction. The shell-model calculations in Ref. [41] employ an extended pairing plus multipole-multipole (EPQQM) model with a frozen ^{78}Ni core and all orbitals in the 28–50 major shell plus $0g_{7/2}$ and $1d_{5/2}$ for protons, and those in the 50–82 major shell plus $1f_{7/2}$ and $2p_{3/2}$ for neutrons.

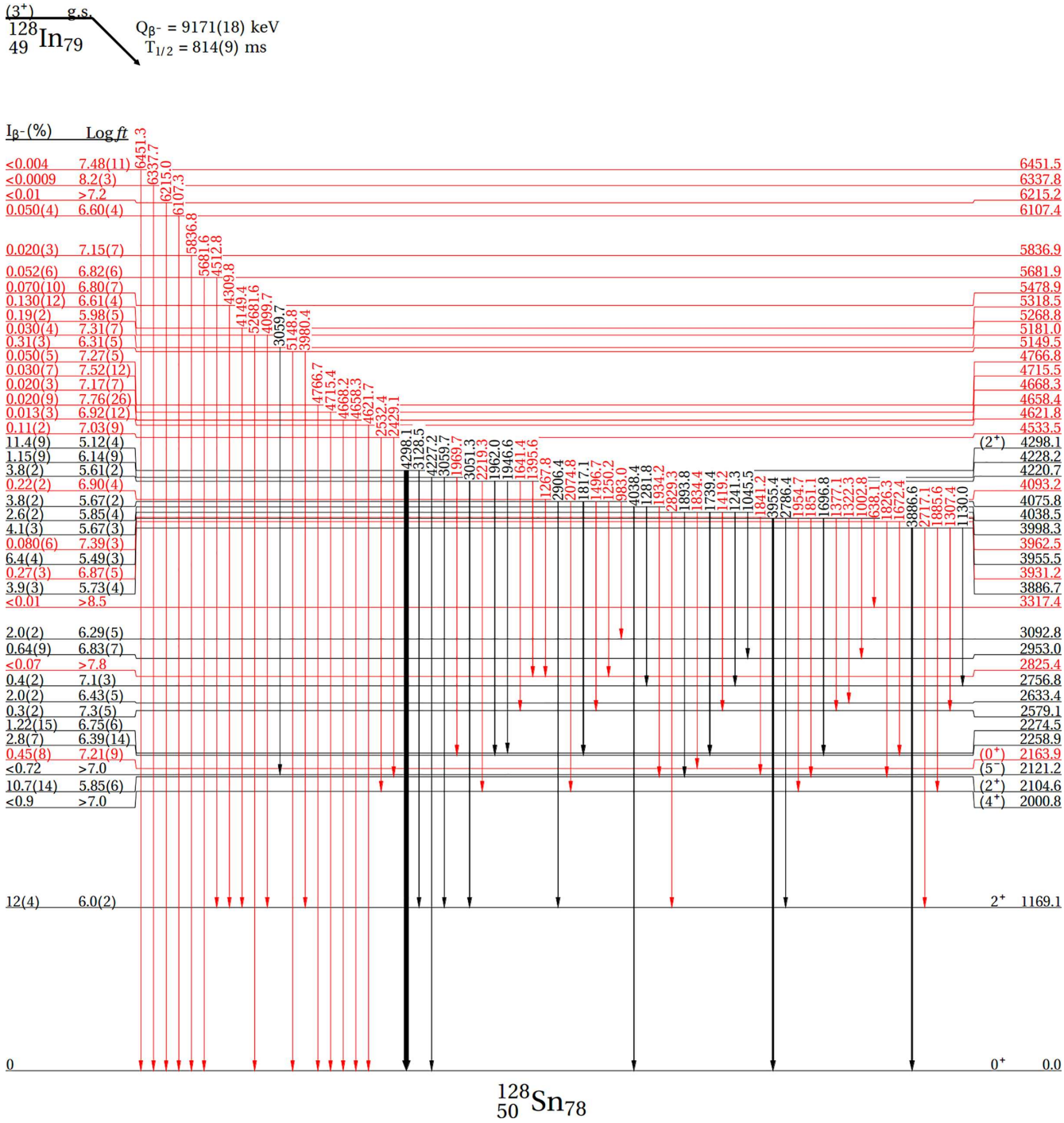

FIG. 6. Level scheme of ^{128}Sn observed following the β decay of the ^{128g}In (3^+) state. Levels and transitions previously identified are colored in black, while those newly identified in this work are highlighted in red. Transition widths are proportional to their relative intensities.

Finally, Cheng *et al.* [42] take a different approach by performing three sets of calculations in the so-called nucleon-pair approximation, a pair-truncation scheme of the shell model based on the generalized seniority scheme. The calculations use the full 50–82 major shell-model space, a truncated nucleon-pair approximation space, and an optimized pair basis where no mixing is considered, respectively.

A. Positive parity states

Considering the dominant $\pi g_{9/2}^{-1}\nu d_{3/2}^{-1}h_{11/2}^{-2}$ configuration of the parent g.s. [41], the most favorable β-decay route is an allowed Gamow-Teller (GT) $\nu g_{7/2} \rightarrow \pi g_{9/2}$ transition [43], which populates positive parity states with a dominant component of the $\nu g_{7/2}^{-1}d_{3/2}^{-1}h_{11/2}^{-2}$ configuration. Since the $g_{7/2}$ is the most bound orbit in the neutron shell (2.44 MeV more

TABLE I. List of γ rays observed following the β decay of ^{128g}In to ^{128}Sn, including transition energies and intensities. The initial and final levels for each connecting transition are also given. Relative γ intensities are normalized to 1000 units for the 1169-keV $2^+ \rightarrow 0^+$ transition. For intensity per 100 decays of the parent ^{128}In multiply by 0.0539(12). γ-ray energies have been corrected for recoil to obtain the energy levels.

E_γ (keV)	I_γ	E_i (keV)	E_f (keV)
120.5(5)	76(12)	2121.2(7)	2000.8(5)
177.4(4)	2.1(3)	2756.8(3)	2579.1(3)
192.1(4)	2.7(4)	2825.4(5)	2633.4(5)
256.9(4)	68(5)	2378.2(8)	2121.2(7)
310.1(4)	0.5(2)	2953.0(4)	2642.8(3)
320.5(4)	13(2)	2579.1(3)	2258.9(4)
351.0(4)	3.0(6)	3092.8(3)	2742.4(5)
368.1(4)	1.67(14)	2642.8(3)	2274.5(4)
377.7(4)	2.2(2)	2378.2(8)	2000.8(5)
384.1(4)	2.3(3)	2642.8(3)	2258.9(4)
447.1(4)	2.8(7)	2825.4(5)	2378.2(8)
449.6(4)	12(2)	3092.8(3)	2642.8(3)
474.5(4)	10(2)	2579.1(3)	2104.6(4)
538.4(3)	25(2)	2642.8(3)	2104.6(4)
574.6(3)	2.1(4)	2953.0(4)	2378.2(8)
584.9(3)	6.7(7)	3227.5(3)	2642.8(3)
638.1(3)	0.85(7)	3955.5(4)	3317.4(5)
642.1(3)	1.90(14)	2642.8(3)	2000.8(5)
652.4(3)	6.2(8)	2756.8(3)	2104.6(4)
704.2(3)	8.2(9)	2825.4(5)	2121.2(7)
763.6(3)	8.6(8)	3520.1(5)	2756.8(3)
778.9(3)	2.0(4)	3421.9(3)	2642.8(3)
831.7(3)	104(10)	2000.8(5)	1169.1(3)
935.6(3)	172(20)	2104.6(4)	1169.1(3)
941.0(3)	24(3)	3520.1(5)	2579.1(3)
966.3(3)	8(2)	2967.1(6)	2000.8(5)
969.0(3)	4.9(13)	3227.5(3)	2258.9(4)
977.3(3)	2.4(2)	3619.8(3)	2642.8(3)
983.0(3)	1.6(3)	4075.8(4)	3092.8(3)
988.4(3)	3.1(5)	3092.8(3)	2104.6(4)
994.8(3)	11(2)	2163.9(5)	1169.1(3)
1002.8(3)	4.7(6)	3955.5(4)	2953.0(4)
1045.5(3)	8.0(10)	3998.3(3)	2953.0(4)
1089.9(3)	153(20)	2258.9(4)	1169.1(3)
1105.4(3)	29(3)	2274.5(4)	1169.1(3)
1123.2(3)	11(2)	3227.5(3)	2104.6(4)
1130.0(3)	5.5(8)	3886.7(5)	2756.8(3)
1136.7(3)	0.42(11)	3241.3(5)	2104.6(4)
1169.1(3)	1000	1169.1(3)	0.0
1241.3(3)	16(2)	3998.3(3)	2756.8(3)
1250.2(3)	3.2(3)	4075.8(4)	2825.4(5)
1261.7(3)	5.3(5)	3520.1(5)	2258.9(4)
1267.8(3)	4.2(5)	4093.2(6)	2825.4(5)
1281.8(3)	15.0(10)	4038.5(5)	2756.8(3)
1307.4(3)	2.2(3)	3886.7(5)	2579.1(3)
1317.5(3)	2.4(2)	3421.9(3)	2104.6(4)
1322.3(3)	1.6(3)	3955.5(4)	2633.4(5)
1357.1(3)	1.2(3)	3520.1(5)	2163.9(5)
1377.1(3)	2.5(3)	3955.5(4)	2579.1(3)
1395.6(3)	10.3(10)	4220.7(3)	2825.4(5)
1410.1(3)	20(2)	2579.1(3)	1169.1(3)
1419.2(3)	10.0(12)	3998.3(3)	2579.1(3)
1464.4(3)	41(4)	2633.4(5)	1169.1(3)
1473.6(3)	37(6)	2642.8(3)	1169.1(3)
1496.7(3)	9.9(9)	4075.8(4)	2579.1(3)
1515.2(3)	7.4(7)	3619.8(3)	2104.6(4)
1573.3(3)	3.2(3)	2742.4(5)	1169.1(3)
1587.7(3)	44(4)	2756.8(3)	1169.1(3)
1641.4(3)	2.7(3)	4220.7(3)	2579.1(3)
1651.9(3)	5.1(6)	3756.5(4)	2104.6(4)
1672.4(3)	2.9(4)	3931.2(4)	2258.9(4)
1696.8(3)	23(2)	3955.5(4)	2258.9(4)
1739.4(3)	35(3)	3998.3(3)	2258.9(4)
1783.9(3)	22(2)	2953.0(4)	1169.1(3)
1817.1(4)	37(4)	4075.8(4)	2258.9(4)
1826.3(4)	2.0(3)	3931.2(4)	2104.6(4)
1834.4(4)	1.3(2)	3998.3(3)	2163.9(5)
1841.2(4)	1.45(13)	3962.5(8)	2121.2(7)
1851.1(4)	3.7(4)	3955.5(4)	2104.6(4)
1885.6(4)	2.1(2)	3886.7(5)	2000.8(5)
1893.8(4)	4.6(4)	3998.3(3)	2104.6(4)
1924.0(4)	18(2)	3092.8(3)	1169.1(3)
1934.2(4)	1.9(4)	4038.5(5)	2104.6(4)
1946.6(4)	7.6(8)	4220.7(3)	2274.5(4)
1954.7(4)	2.4(4)	3955.5(4)	2000.8(5)
1962.0(4)	20(2)	4220.7(3)	2258.9(4)
1969.7(4)	7.1(9)	4228.2(4)	2258.9(4)
2010.9(4)	1.6(3)	3180.0(5)	1169.1(3)
2058.7(4)	1.9(2)	3227.5(3)	1169.1(3)
2074.8(4)	1.1(4)	4075.8(4)	2000.8(5)
2104.6(4)	111(11)	2104.6(4)	0.0
2148.3(4)	0.95(12)	3317.4(5)	1169.1(3)
2219.3(4)	1.2(3)	4220.7(3)	2000.8(5)
2258.8(4)	50(5)	2258.9(4)	0.0
2275.1(4)	3.0(3)	2274.5(4)	0.0
2351.3(4)	27(3)	3520.1(5)	1169.1(3)
2429.1(4)	1.2(2)	4533.5(4)	2104.6(4)
2450.9(4)	2.6(3)	3619.8(3)	1169.1(3)
2532.4(5)	0.8(3)	4533.5(4)	2000.8(5)
2578.9(5)	16.0(14)	2579.1(3)	0.0
2717.1(5)	3.0(7)	3886.7(5)	1169.1(3)
2786.4(5)	10.7(3)	3955.5(4)	1169.1(3)
2829.3(5)	2.9(3)	3998.3(3)	1169.1(3)
2906.4(5)	17(2)	4075.8(4)	1169.1(3)
3051.3(5)	28(3)	4220.7(3)	1169.1(3)
3059.7(5)	5.78(10)	4228.2(4)	1169.1(3)
3059.7(5)	0.52(7)	5181.0(9)	2121.2(7)
3091.7(5)	3.4(4)	3092.8(3)	0.0
3128.5(5)	15.0(14)	4298.1(6)	1169.1(3)
3226.9(5)	12.9(13)	3227.5(3)	0.0
3520.0(6)	278(30)	3520.1(5)	0.0
3619.6(6)	8.3(9)	3619.8(3)	0.0
3756.2(6)	2.0(2)	3756.5(4)	0.0
3886.6(6)	60(6)	3886.7(5)	0.0
3955.4(6)	70(7)	3955.5(4)	0.0
3980.4(6)	5.4(6)	5149.5(7)	1169.1(3)
4038.4(6)	31(3)	4038.5(5)	0.0
4099.7(6)	3.4(3)	5268.8(7)	1169.1(3)

TABLE I. (*Continued.*)

E_γ (keV)	I_γ	E_i (keV)	E_f (keV)
4149.4(6)	2.5(3)	5318.5(7)	1169.1(3)
4227.2(6)	8.4(9)	4228.2(4)	0.0
4298.1(6)	198(20)	4298.1(6)	0.0
4309.8(6)	1.3(2)	5478.9(7)	1169.1(3)
4512.8(6)	0.77(12)	5681.9(6)	1169.1(3)
4621.7(6)	0.24(6)	4621.8(6)	0.0
4658.3(6)	0.4(2)	4658.4(6)	0.0
4668.2(6)	0.4(1)	4668.3(6)	0.0
4715.4(5)	0.59(13)	4715.5(5)	0.0
4766.7(5)	0.94(11)	4766.8(5)	0.0
5148.8(5)	0.42(6)	5149.5(7)	0.0
5269.1(5)	0.17(10)	5268.8(7)	0.0
5681.6(5)	0.19(4)	5681.9(6)	0.0
5836.8(4)	0.39(7)	5836.9(4)	0.0
6107.3(4)	0.95(9)	6107.4(4)	0.0
6215.0(4)	0.12(2)	6215.2(4)	0.0
6337.7(4)	0.017(7)	6337.8(4)	0.0
6451.3(3)	0.08(2)	6451.5(3)	0.0

compared to the $d_{3/2}$ [43]), a high excitation energy can be expected for this configuration. The strong β population observed to high-energy levels above 3 MeV, such as the 3520- and 4298-keV states with $\log ft$ values equal to 5.18(3) and 5.12(4), respectively, is likely due to this GT transition. These states are tentatively assigned (2^+) spin-parity. In fact, the 2^+ states above 3.2 MeV may contain admixtures of other neutron-hole wave functions from the $s_{1/2}$, $d_{5/2}$, and $g_{7/2}$ orbitals. For example, the shell-model calculations in Ref. [41] obtain that the 2^+ state at 4298 keV has a 57% contribution from the $\nu h_{11/2}^{-2} d_{3/2}^{-1} g_{7/2}^{-1}$ and 14% from the $\nu h_{11/2}^{-2} d_{3/2}^{-1} s_{1/2}^{-1}$ configurations. This indicates that, while the primary configuration is still $\nu h_{11/2}^{-2} d_{3/2}^{-1} g_{7/2}^{-1}$, there is significant mixing

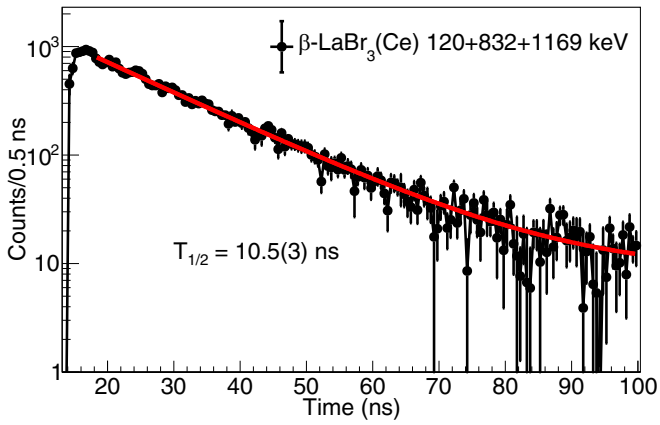

FIG. 7. Time-delayed spectrum between the β detector and either of the two $LaBr_3$(Ce) detectors for $\beta\gamma(t)$ events. This distribution is built by adding up the 120-, 832-, and 1169-keV transitions in the $LaBr_3$(Ce) detectors. A time window gate corresponding to the ^{128}In half-life was imposed to reduce the background. The lifetime was obtained by a χ^2 minimization of the time distribution to an exponential decay with a constant background component.

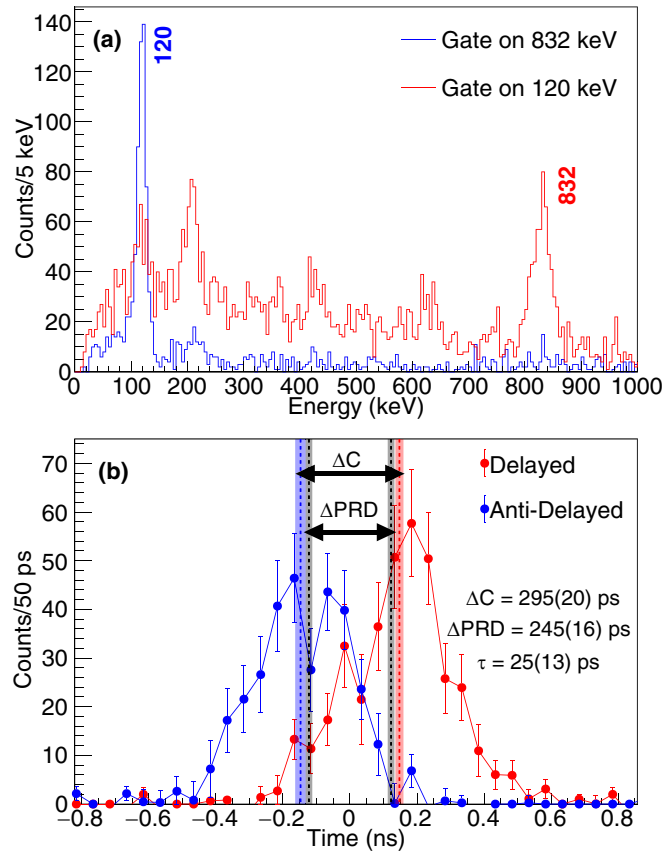

FIG. 8. Energy spectra recorded in the $LaBr_3$(Ce) start detector after gating in the 120 and 832-kev on the stop $LaBr_3$(Ce) detector respectively (a). Time delay distributions between the two $LaBr_3$(Ce) detectors for $\gamma\gamma(t)$ events (b). Depending on the selected γ transition in the start and stop detectors, either the delayed or the antidelayed distributions are derived. The centroid is shown with a dashed line, while the shaded area represents its uncertainty. The centroid shift measured between the delayed and antidelayed time spectra (ΔC), is caused by the lifetime of the level and the shift in the prompt response difference (ΔPRD) [22,23,32,34].

with other configurations, which contributes to increasing the energy of the state.

Turning now to the 2^+ states below 3.2 MeV, they are dominated by the $\nu h_{11/2}^{-2} d_{3/2}^{-2}$ configuration [41]. In this energy range, the neutron orbitals $h_{11/2}$ and $d_{3/2}$ are close in energy, which facilitates their coupling to 2^+ states. The direct β-decay feeding to these 2^+ states is much more suppressed in comparison to those located above, their $\log ft$ values being consistently higher than 5.8, which does not support a GT character [30]. The hindrance is even more pronounced for the first 4^+ state, with $\log ft > 7$. The origin of this strong suppression can be the small overlap between the initial and final state configurations, which, in the single-particle picture, would require a second-forbidden $\nu d_{3/2} \rightarrow \pi g_{9/2}$ transition to connect them. However, the 1.5 MeV gap between the highest observed level and the neutron separation energy suggests the possibility of unobserved feeding into higher-lying states. These states could feed the 2^+ levels through high-energy

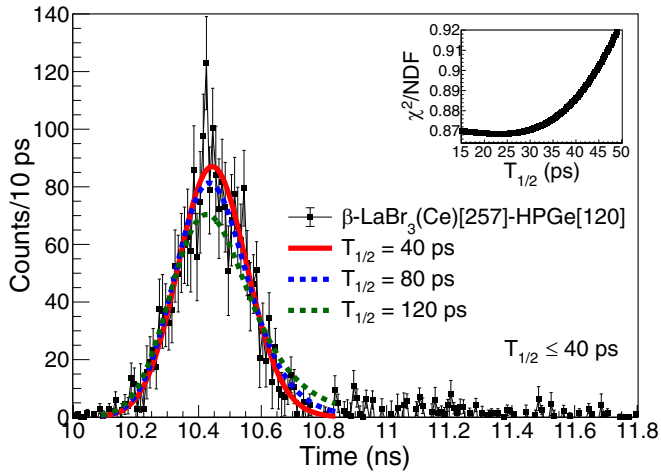

FIG. 9. Time-delayed $\beta\gamma\gamma(t)$ spectrum between the β and the $LaBr_3$(Ce) detectors selected by the 257-keV transition. An extra condition was required in the 120-keV γ transition in the HPGe detectors. The lifetime was obtained from a χ^2 minimization of the distribution to a Gaussian convoluted with exponential function. The inset plot shows the χ^2/NDF vs half-life dependence. To show the robustness of the fitting method, half-lives of 80 and 120 ps with a Gaussian prompt with fixed width are shown by the blue and green dotted lines, respectively.

γ-ray cascades that remain undetected due to experimental limitations [44].

In this work the first lifetime measurement for the (4^+) state at 2001 keV has been provided, from which an experimental $B(E2;\ 4^+ \rightarrow 2^+) = 2.1(^{+2.3}_{-0.7})$ W.u. has been deduced. Figure 11 shows experimental $B(E2;\ 2^+ \rightarrow 0^+)$ and $B(E2;\ 4^+ \rightarrow 2^+)$ reduced transition probabilities for the even-even Sn isotopes compared to calculations available in the literature. Shell-model calculations in Ref. [38] are in agreement with the experimental values. More recent calculations for $^{126-130}$Sn [39,42] are also consistent with the experimental results and seem to reproduce the new $B(E2;\ 4^+ \rightarrow 2^+)$ within the large experimental uncertainty. The observed trend varies significantly depending on the type of calculation and the model employed. Data about the yet to be experimentally measured $B(E2;\ 4^+ \rightarrow 2^+)$ values in the neighboring ^{126}Sn and ^{130}Sn will help us to understand the systematics of $E2$ transition strengths approaching ^{132}Sn.

The new level established at 2164 keV (see Fig. 4) has been tentatively assigned spin-parity (0^+), based on its deexciting pattern, and is in agreement with the systematics of the 0^+_2 states in even Sn nuclei; see Fig. 10. This is consistent with the shell-model calculations presented in Ref. [40], which predict an energy of 2159 keV for the 0^+_2 level with the main $\nu h^{-4}_{11/2}$ configuration having an amplitude of 47%.

B. Negative parity states

The close-lying levels of $\nu h_{11/2}$ and $\nu d_{3/2}$ orbitals lead to the existence of low-lying negative parity states based on the $\nu h^{-1}_{11/2} d^{-1}_{3/2}$ coupling, leading to a $J^\pi = (4, 5, 6, 7)^-$ multiplet. One expects a sizable direct feeding to members of the multiplet in the β-decay transition from the (3^+) ground state in ^{128}In. More particularly, the population of the 4^- state should be observed due to the predominance of the first-forbidden $\nu h_{11/2} \rightarrow \pi g_{9/2}$ transition [43]. The 5^- and 7^- members are assigned to the 2121- and 2091-keV experimental states, respectively, while the 4^- and 6^- states remain unidentified. The systematics of even-even tin isotopes in Fig. 10 and the shell-model calculations [42] indicate their positions in the 2–3 MeV range.

An interesting result emerges from the observed direct feeding to the 2378-keV level in the β decay of ^{128}In (3^+) g.s., with an $I_\beta = 3.7(2)\%$ and $\log ft = 6.23(2)$. This state was formerly assigned spin-parity (7^-) [6], which would imply a third-forbidden unique β transition. This is difficult to reconcile with the experimental observation, even if populating high-energy γ transitions are missed. Moreover, the upper limit of 40-ps half-life indicates that the 257-keV γ ray that connects this state to the 2121-keV (5^-) level is predominantly of $M1$ character. A pure $E2$ multipolarity required by a potential $(7^-) \rightarrow (5^-)$ transition would yield an unrealistic $B(E2) \geqslant 304$ W.u. Additionally, a small branching ratio for a 378-keV transition connecting to the 2001-keV (4^+) state was found. Considering the half-life upper limit and the branching ratio, a lower limit of $B(E1) \geqslant 4 \times 10^{-6}$ W.u. is obtained, which is compatible with the $B(E1) = 1.31(4) \times 10^{-5}$ W.u. measured for the $(5^-) \rightarrow (4^+)$ transition. The evidence leads us to interpret the 2378-keV state as the missing 4^- member of the $\nu d^{-1}_{3/2} h^{-1}_{11/2}$ multiplet—see Fig. 10—and to propose a (4^-) assignment for this level.

V. CONCLUSIONS

A detailed investigation of the excited state structure of ^{128}Sn, populated exclusively through the β decay of ^{128g}In, was conducted. Utilizing high-resolution γ-ray spectroscopy and advanced fast-timing techniques at the ISOLDE Decay Station, the previously known β decay scheme from ^{128g}In

TABLE II. Level lifetimes and reduced transition probabilities for transitions in ^{128}Sn. The spin assignments for the initial and final level follow Ref. [9], except for the (4^-) level, which is proposed in this work. The $B(X\lambda)$ were calculated from the lifetimes and branching ratios obtained in this work, using conversion coefficients taken from [31] and assuming pure multipolarities as indicated.

E_i (keV)	J^Π_i	τ	E_f (keV)	J^Π_f	E_γ (keV)	$X\lambda$	$B(X\lambda)$ (W.u.)
2121	(5^-)	15.2(4) ns	2001	(4^+)	120	$E1$	$1.31(4) \times 10^{-5}$
2378	(4^-)	$\leqslant$57 ps	2121	(5^-)	257	$M1$	$\geqslant 3 \times 10^{-2}$
			2001	(4^+)	378	$E1$	$\geqslant 4 \times 10^{-6}$
2001	(4^+)	25(13) ps	1169	(2^+)	832	$E2$	$2.1(^{+2.3}_{-0.7})$

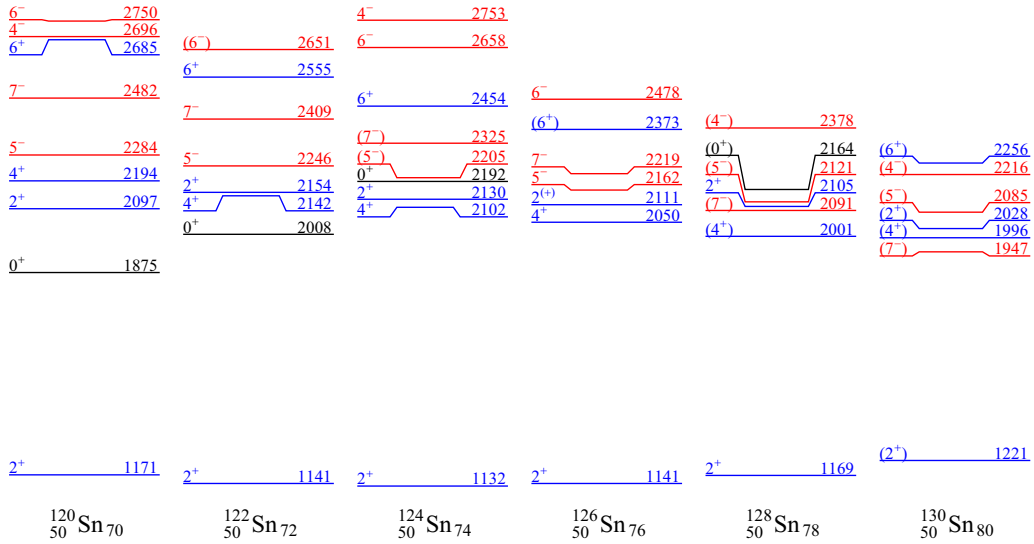

FIG. 10. Energies of excited states in the even-even Sn isotopes. Positive-parity states are shown in blue and negative-parity states in red. The 0_2^+ states are represented in black. The 0_1^+ ground states are not plotted for the sake of clarity. Data are taken from Ref. [9] and from the present work for ^{128}Sn.

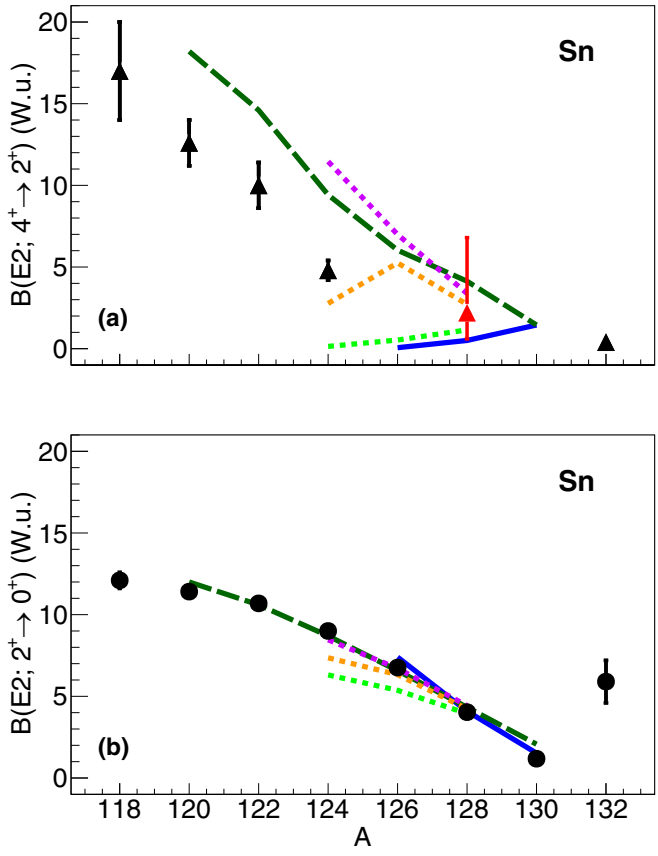

FIG. 11. Experimental reduced transition probabilities in W.u. for the $4^+ \rightarrow 2^+$ (a) and $2^+ \rightarrow 0^+$ (b) transitions in the even Sn isotopes, taken from Ref. [9]. The $B(E2; 4^+ \rightarrow 2^+)$ value for ^{128}Sn measured in this work is plotted in red. Theoretical calculations are shown with lines: Holt *et al.* solid (blue) [38], Teruya *et al.* dashed (dark green) [39] and Cheng *et al.* dotted (light green, orange, and violet) [42].

(3^+) to ^{128}Sn was disentangled and significantly expanded. A total of 81 new γ transitions and 30 new levels were identified, providing a comprehensive update to the ^{128}Sn level scheme.

The lifetime of the (4^+) state at 2001 keV was measured for the first time. The experimental $B(E2; 4^+ \rightarrow 2^+) = 2.1(^{+2.3}_{-0.7})$ W.u. is consistent within the large experimental uncertainty with the shell-model predictions and with the systematics of the neighboring even-even Sn isotopes. The reassessment of the half-life of the (5^-) state at 2121 keV yielded $T_{1/2} = 10.5(3)$ ns, more than two standard deviations away from the adopted value. Additionally, the lifetime of the 2378 keV level was measured, establishing an upper limit for the half-life of 40 ps. This level deexcites via a 257-keV γ ray to the (5^-) level at 2121 keV and via a 378-keV γ ray to the 2001-keV (4^+) level. The derived reduced transition probabilities, $B(M1) \geqslant 3 \times 10^{-2}$ W.u. for the 257-keV transition and $B(E1) \geqslant 4 \times 10^{-6}$ W.u. for the 378-keV transition, support a tentative spin-parity assignment of (4^-) for the 2378-keV state.

ACKNOWLEDGMENTS

We thank the ISOLDE technical teams for providing excellent experimental conditions and we acknowledge the support of the ISOLDE Collaboration and of the European Union's EURO-LABS research and innovation program under Grant Agreement No. 101057511. This research was funded by the Spanish MCIN/AEI/10.13039/501100011033 via RTI2018-098868-B-I00, PRE2019-091450, PID2021-126998OB-I00, PID2022-138297NB-C21, PID2022-140162NB-I00, and and Severo Ochoa CEX2023-001292-S grants. J.B. acknowledges support from the Margarita Salas Fellowship, CT31/21, at the Complutense University of Madrid, funded by the Spanish MIU and European Union-Next-Generation funds. A.I. acknowledges funding from the European Union's Horizon 2020 research and innovation program under the

Marie Skłodowska-Curie Grant Agreement No. 847635. S.L. acknowledges support from the European Union–Next Generation EU, the National Recovery and Resilience Plan of the Republic of Bulgaria, Project BG-RRP-2.004-0008-C01. Ir.V. is supported by the Bulgarian National Science Fund under Contract No. KP-06-N68/8. We also acknowledge support from Grupo de Física Nuclear-UCM Ref. 910059; from the Comunitat Valenciana Prometeo CIPROM/2022/9 grant; from the Research Foundation Flanders (FWO, Belgium); from the BOF KU Leuven (C14/22/104) and the BOF KU Leuven (GOA/2015/010); from the Polish National Science Center under Grants No. 2020/39/B/ST2/02346 and No. 2024/53/N/ST2/03168; from the Polish Ministry of Science and Higher Education under Contract No. 2021/WK/07 and "Excellence Initiative–Research University" program; from the German BMBF under Contract No. 05P21PKCI1 and Verbundprojekt 05P2021; from the Academy of Finland Project No. 354968; from the United Kingdom Science and Technology Facilities Council under Grants No. ST/V001108/1, No. ST/P004598/1 and No. ST/V001027/1; from the Slovak Research and Development Agency (Contract No. APVV-22-0282); and from the Romanian IFA Grant CERN/ISOLDE and the Nucleu Project No. PN 23 21 01 02.

DATA AVAILABILITY

The data that support the findings of this article are not publicly available. The data are available from the authors upon reasonable request.

[1] K. L. Jones, A. S. Adekola, D. W. Bardayan, J. C. Blackmon, K. Chae, K. Chipps, J. Cizewski, L. Erikson, C. Harlin, R. Hatarik *et al.*, Nature (London) **465**, 454 (2010).
[2] D. Rosiak, M. Seidlitz, P. Reiter, H. Naïdja, Y. Tsunoda, T. Togashi, F. Nowacki, T. Otsuka, G. Colò, K. Arnswald *et al.* (MINIBALL Collaboration), Phys. Rev. Lett. **121**, 252501 (2018).
[3] J. Benito, L. M. Fraile, A. Korgul, M. Piersa, E. Adamska, A. Andreyev, R. Álvarez-Rodríguez, A. Barzakh, G. Benzoni, T. Berry *et al.* (IDS Collaboration), Phys. Rev. C **102**, 014328 (2020).
[4] L. Coraggio, A. Covello, A. Gargano, and N. Itaco, Phys. Rev. C **87**, 034309 (2013).
[5] M. Wang, W. J. Huang, F. G. Kondev, G. Audi, and S. Naimi, Chin. Phys. C **45**, 030003 (2021).
[6] B. Fogelberg and P. Carlé, Nucl. Phys. A **323**, 205 (1979).
[7] B. Fogelberg, K. Heyde, and J. Sau, Nucl. Phys. A **352**, 157 (1981).
[8] B. S. Wang, S. A. Caldwell, N. D. Scielzo, A. Czeszumska, J. A. Clark, G. Savard, A. Aprahamian, M. T. Burkey, C. J. Chiara, J. Harker *et al.*, Phys. Rev. C **101**, 025806 (2020).
[9] National Nuclear Data Center (NNDC), http://www.nndc.bnl.gov.
[10] D. Nesterenko, A. Kankainen, J. Kostensalo, C. Nobs, A. Bruce, O. Beliuskina, L. Canete, T. Eronen, E. Gamba, S. Geldhof *et al.*, Phys. Lett. B **808**, 135642 (2020).
[11] C. Izzo, J. Bergmann, K. Dietrich, E. Dunling, D. Fusco, A. Jacobs, B. Kootte, G. Kripkó-Koncz, Y. Lan, E. Leistenschneider *et al.*, Phys. Rev. C **103**, 025811 (2021).
[12] S. Pietri, A. Jungclaus, M. Górska, H. Grawe, M. Pfützner, L. Cáceres, P. Detistov, S. Lalkovski, V. Modamio, Z. Podolyák *et al.*, Phys. Rev. C **83**, 044328 (2011).
[13] Ł. W. Iskra, R. Broda, R. V. F. Janssens, J. Wrzesiński, B. Szpak, C. J. Chiara, M. P. Carpenter, B. Fornal, N. Hoteling, F. G. Kondev *et al.*, Phys. Rev. C **89**, 044324 (2014).
[14] U. Köster, O. Arndt, E. Bouquerel, V. Fedoseyev, H. Frånberg, A. Joinet, C. Jost, I. Kerkines, and R. Kirchner (The TARGISOL Collaboration), Nucl. Instrum. Methods Phys. Res., Sect. B **266**, 4229 (2008).
[15] K. L. Kratz, H. Gabelmann, P. Möller, B. Pfeiffer, H. Ravn, and A. Wöhr (ISOLDE Collaboration), Z. Phys. A **340**, 419 (1991).
[16] E. Bouquerel, R. Catherall, M. Eller, J. Lettry, S. Marzari, and T. Stora (ISOLDE Collaboration), Eur. Phys. J. Spec. Top. **150**, 277 (2007).
[17] V. Fedosseev, K. Chrysalidis, T. D. Goodacre, B. Marsh, S. Rothe, C. Seiffert, and K. Wendt, J. Phys. G: Nucl. Part. Phys. **44**, 084006 (2017).
[18] U. Köster, V. Fedoseyev, A. Andreyev, U. Bergmann, R. Catherall, J. Cederkäll, M. Dietrich, H. De Witte, D. Fedorov, L. M. Fraile *et al.*, Nucl. Instrum. Methods Phys. Res., Sect. B **204**, 347 (2003).
[19] M. Llanos-Expósito, L. M. Fraile, J. Benito, J. Acosta, A. Algora, B. Andel, A. Andreyev, S. Antalic, R. Bark, C. Bernerd *et al.*, Acta Phys. Pol. B Proc. Suppl. **17** (2024).
[20] V. Vedia, H. Mach, L. M. Fraile, J. M. Udías, and S. Lalkovski, Nucl. Instrum. Methods Phys. Res., Sect. A **795**, 144 (2015).
[21] V. Vedia, M. Carmona-Gallardo, L. M. Fraile, H. Mach, and J. M. Udías, Nucl. Instrum. Methods Phys. Res., Sect. A **857**, 98 (2017).
[22] H. Mach, R. Gill, and M. Moszyński, Nucl. Instrum. Methods Phys. Res., Sect. A **280**, 49 (1989).
[23] J.-M. Régis, G. Pascovici, J. Jolie, and M. Rudigier, Nucl. Instrum. Methods Phys. Res., Sect. A **622**, 83 (2010).
[24] L. M. Fraile, J. Phys. G: Nucl. Part. Phys. **44**, 094004 (2017).
[25] F. Kondev, M. Wang, W. Huang, S. Naimi, and G. Audi, Chin. Phys. C **45**, 030001 (2021).
[26] P. Reeder, R. Warner, M. Edmiston, R. Gill, and A. Piotrowski, in *Nuclei Off the Line of Stability* (ACS, Washington, 1985).
[27] G. Rudstam, K. Aleklett, and L. Sihver, At. Data Nucl. Data Tables **53**, 1 (1993).
[28] O. Hall, T. Davinson, A. Estrade, J. Liu, G. Lorusso, F. Montes, S. Nishimura, V. Phong, P. J. Woods, J. Agramunt *et al.*, Phys. Lett. B **816**, 136266 (2021).
[29] H. Bateman, Proc. Lond. Math. Soc. **2**, 223 (1910).
[30] S. Turkat, X. Mougeot, B. Singh, and K. Zuber, At. Data Nucl. Data Tables **152**, 101584 (2023).
[31] T. Kibédi, T. Burrows, M. Trzhaskovskaya, P. Davidson, and C. Nestor, Nucl. Instrum. Methods Phys. Res., Sect. A **589**, 202 (2008).
[32] M. Moszyński and H. Mach, Nucl. Instrum. Methods Phys. Res., Sect. A **277**, 407 (1989).

[33] J. Benito, Gamma and fast-timing spectroscopy of exotic tin isotopes around ^{132}Sn, Ph.D. thesis, Universidad Complutense de Madrid, Madrid, 2020.
[34] Z. Bay, Phys. Rev. **77**, 419 (1950).
[36] N. Bernier, Decay spectroscopy of neutron-rich cadmium around the $N = 82$ shell closure, Ph.D. thesis, University of British Columbia, Vancouver, 2018.
[37] A. Scherillo, J. Genevey, J. A. Pinston, A. Covello, H. Faust, A. Gargano, R. Orlandi, G. S. Simpson, I. Tsekhanovich, and N. Warr, Phys. Rev. C **70**, 054318 (2004).
[38] A. Holt, T. Engeland, M. Hjorth-Jensen, and E. Osnes, Nucl. Phys. A **634**, 41 (1998).
[39] E. Teruya, N. Yoshinaga, K. Higashiyama, and A. Odahara, Phys. Rev. C **92**, 034320 (2015).
[40] E. E. Peters, A. E. Stuchbery, A. Chakraborty, B. P. Crider, S. F. Ashley, A. Kumar, M. T. McEllistrem, F. M. Prados-Estévez, and S. W. Yates, Phys. Rev. C **99**, 064321 (2019).
[41] H.-K. Wang, Z.-H. Li, Y.-B. Wang, and B. Jiang, Phys. Lett. B **833**, 137337 (2022).
[42] Y. Y. Cheng, C. Qi, Y. M. Zhao, and A. Arima, Phys. Rev. C **94**, 024321 (2016).
[43] J. Benito, L. M. Fraile, A. Korgul, M. Piersa-Siłkowska, A. Jaries, M. Stryjczyk, E. Adamska, R. Álvarez-Rodríguez, A. Andreyev, A. Barzakh *et al.* (IDS and IGISOL Collaboration), Phys. Rev. C **110**, 014328 (2024).
[44] J. Hardy, L. Carraz, B. Jonson, and P. Hansen, Phys. Lett. B **71**, 307 (1977).